scientific reports

Check for updates

OPEN

Plant-derived extracellular vesicles for itraconazole delivery across the blood-brain barrier for potential glioblastoma treatment

Naznin Bhom[1], Poornima Ramburrun[1], Khonzisizwe Somandi[1,2] & Yahya E. Choonara[1,2]✉

Background A major challenge in central nervous system disorders such glioblastoma includes the presence of a blood-brain barrier which restricts the delivery of therapeutic agents to the brain, thereby limiting the effectiveness of most conventional treatments. Moreover, the discovery of novel drugs for glioblastoma has been limited hence drug repurposing has gained traction leveraging existing drugs like itraconazole. Plant-derived extracellular vesicles (PDEVs) have potential as a natural pharmaceutical delivery system owing to their therapeutic capabilities. These PDEVs may be a good candidate for blood-brain barrier permeation due to their biomolecular composition and high drug loading efficiency of itraconazole. In this work, PDEVs isolated from aloe aborescens (aloe), Zingiber officinale (ginger) and Nigella sativa seeds [black cumin seeds (BCS)] were compared in terms of their physicochemical properties, drug release kinetics, cytotoxicity, cellular uptake in glioblastoma cells and BBB permeability. **Results** All PDEVs displayed nanoscale sizes ranging from 103.5 to 141 nm with negative surface charge and a spherical morphological shape observed via SEM. The drug release kinetics was assessed using different mathematical models depicting the PDEVs prolonged drug release with < 50% releasing over 21 days. The cytotoxicity studies showed that the PDEVs resulted in a higher cell viability in the non-cancerous cell line compared to A172 glioblastoma cell line. The cellular internalization of the drug showed poor uptake of blank PDEVs compared to loaded PDEVs in glioblastoma cells. The BBB permeability test showed that ginger and aloe EVs permeated the BBB whilst BCS blank and loaded EVs did not permeate the BBB. **Conclusions** This delivery system improves the ability of plant-derived extracellular vesicles to cross the blood-brain barrier, addressing a key challenge in delivering treatments to the brain. Through successful encapsulation of itraconazole, it paves the way for glioblastoma treatment by repurposing itraconazole with improved efficacy and reduced side effects. Furthermore, this can be incorporated in various drug delivery vehicles depending on the route of administration and therapeutic outcome i.e. intranasal, intravenous, or oral route. Future studies focus on determining the composition of PDEVs to enable engineering strategies for next generation targeting via surface modification.

Keywords Blood-brain barrier, Plant-derived extracellular vesicles, Glioblastoma, Drug repurposing, Drug delivery, Itraconazole

The blood-brain barrier (BBB) constitutes brain endothelial cells surrounded by pericytes, astrocytes, neurons and microglial cells that regulates the permeability of substances moving across the neurovascular region[1,2]. The BBB interface facilitates the transport of lipophilic molecules (< 400 Da) into the neurovascular region, critically important for advanced drug delivery for brain tumours (Glioblastoma Multiforme – GBM). While selective permeability of the BBB is essential to maintain brain homeostasis, it is a significant challenge for drug delivery to treat CNS conditions such as GBM. Hence, BBB-targeting delivery systems has become a major focus area of innovation.

[1]Wits Advanced Drug Delivery Platform Research Unit, Department of Pharmacy and Pharmacology, School of Therapeutic Sciences, Faculty of Health Sciences, University of the Witwatersrand, 7 York Road Parktown,, Johannesburg 2193, South Africa. [2]Wits Infectious Diseases and Oncology Research Institute, Faculty of Health Sciences, University of the Witwatersrand, 7 York Road Parktown,, Johannesburg 2193, South Africa. ✉email: yahya.choonara@wits.ac.za

GBM is a common primary brain malignancy (a grade IV glioma) with a five-year survival rate of < 5% according to the World Health Organization (WHO) classification[3]. Current treatment of GBM includes adjuvant therapies such as radiotherapy and chemotherapy however their efficacy is limited. The treatment is limited due to the frequent mutation of GBM cells and the BBB hindering the permeation of the chemotherapeutic drugs, thus lowering its efficiency on GBM cells[4].

In the search of alternative non-invasive approaches of traversing the BBB to effectively treat GBM, research is increasingly moving towards exploring the use of extracellular vesicles (EVs) as a delivery tool. EVs are natural-derived nanoparticles from either cells, biological fluids or plant material, having a lipid-bilayer and biological composition that can regulate intercellular communication (the secrotome)[5,6]. EVs range in size from 30 to 150 nm and their inherent function is to transfer endogenous molecules as cargo to other receiving cells[7]. They have also been successfully investigated as a promising biomarker in the early diagnosis of infectious disease, and autoimmune disorders[8].

EVs are assembled from a complex mixture of lipids, membrane/inner vesicular proteins, RNAs and integrins that facilitates long-range transfer across different cells or tissues through the systemic circulation[6,9]. The lipid bilayer of EVs can penetrate the BBB to transport therapeutic molecules to biological targets across the BBB[10]. Among the various types of EVs, Plant-Derived Extracellular Vesicles (PDEVs) have gained significant attention for their safety, scalability, and eco-friendly production[11]. Unlike animal-derived counterparts, PDEVs are less likely to trigger immune responses and can be produced in large quantities with minimal cost as an attractive delivery platform for CNS drugs[12,13].

In particular, plants such as *Aloe aborescens* (aloe), *Zingiber officinale* (ginger) and *Nigella sativa* (black cumin seeds), have been used historically as phytomedicines[14–16]. For example, the leaves of aloe are reported to have chromone or anthrone derivatives potentially providing antioxidant, anti-tumour, and antifungal activities[17]. Ginger contains gingerols, a major polyphenol with anti-inflammatory, antimicrobial and anticancer activities and black cumin seeds contain thymoquinone, a major active chemical component with anti-inflammatory, and neuroprotective activity[18,19].

PDEVs have emerged as promising nanocarriers for the delivery of lipophilic drug due to the high loading efficiency and biocompatibility[20]. Among these, itraconazole (ITZ) is a highly lipophilic antifungal agent which has garnered attention for its potential in anti-cancer activity, making it a compelling candidate for repurposing strategies. Despite decades of research, the discovery of novel drugs for GBM has been limited hence drug repurposing has gained traction as a viable and time-efficient approach leveraging existing drugs like ITZ[21,22]. Recent studies suggest that ITZ has promising anti-angiogenic and anti-tumour activity, a potential candidate for repurposing to treat GBM[10,23]. In previous published reports, ITZ inhibited the hedgehog signalling pathway and angiogenesis[10]. However, its clinical application for CNS conditions is limited by its poor aqueous solubility, low bioavailability, and the BBB due to its high molecular weight and significantly protein bound (albumin)[24]. Hence, encapsulating ITZ within PDEVs may provide a novel strategy to overcome the current limitations for BBB targeted drug delivery to enhance its bioavailability for GBM to extort its promising angiogenesis and anti-tumour activity.

Despite growing interest in targeted drug delivery for GBM, there remains a significant gap in understanding the potential for PDEVs to facilitate targeted drug transport across the BBB. While ITZ has shown promising anticancer activity, its full therapeutic potential can be unlocked by using PDEVs to overcome its poor solubility, systemic toxicity and low permeability across the BBB. PDEVs are neurocompatible materials and scalable. However, there is a significant gap in exploring the use of PDEVs to encapsulate and deliver repurposed drugs such as ITZ to treat GBM. The synergistic potential of combining ITZ with the biopharmaceutical advantages of PDEVs remains underexplored.

Therefore this study focuses on bridging this gap by extracting PDEVs from three common plant sources, *Aloe aborescens* (aloe), *Zingiber officinale* (ginger) and *Nigella sativa* seeds [black cumin seeds (BCS)], and further characterize their pharmaceutical properties including, drug loading capacity, provide controlled drug release, cytotoxicity in GBM cells over a non-cancerous cell line, internalization into GBM cells and the ability to permeate the BBB. This approach provides a novel platform to enhance the efficiency of ITZ with effective BBB permeation and to fully unlock the repurposed anti-tumour activity of ITZ for GBM treatment.

Materials and methods

Materials

Aloe aborescens (aloe), *Zingiber officinale* (ginger) and *Nigella sativa* seeds (black cumin seeds) were purchased from different local nurseries and supermarkets (Johannesburg, South Arica). Itraconazole (ITZ) was purchased from DB Fine Chemicals (South Africa). Dichloromethane (DCM), HPLC grade acetonitrile, triethylamine (TEA), HPLC grade methanol, Sodium lauryl sulphate (SLS), Foetal bovine serum (FBS), Penicillin-Streptomycin (10000 U/ml), 5-dimethylthiazole-2-yl)−2,5-diphenyltetrazolium bromide dye (MTT), 0.25% w/v trypsin, and Dulbecco's Modified Eagle Medium (DMEM), Fluorescein Isothiocyanate (FITC), DAPI (4',6-diamidino-2-phenylindole) were purchased from Sigma (Sigma- Aldrich, Missouri, USA). Glioblastoma (A172) cells and keratinocytes (HaCat) were purchased from the American Type Culture Collection (ATCC) (Rockville, MD, USA). A Parallel Artificial Membrane Permeability Assay-BBB Kit (PMBBB) was purchased from BioAssay™ Systems, Hayward, CA, USA. All reagents and chemicals used were of high analytical grade.

PDEVs sample collection, extraction and purification

Plant-derived EVs (PDEVs) were extracted from ginger rhizomes, rinds of aloe and black cumin seeds (BCS). They were selected because of their intrinsic properties and are consumed for several therapeutic purposes. The following plants were weighed, washed with milli-Q water and, after the excess water was removed, the samples were homogenized in phosphate-buffered saline (PBS, pH = 7.4) at a ratio of 1:3 (w/v) using a high-

speed blender (5000 Series Blender, Phillips, South Africa) to obtain the plant homogenate. The homogenate was further subjected to extraction of PDEVs as shown in Fig. 1.

To remove the large particles and the cellular debris, the homogenate was collected in centrifuge tubes and centrifuged (Eppendorf Centrifuge 5810R, Hamburg, Germany) at 1000 x g for 10 min, 2000 x g for 20 min and 3000 x g for 30 min at 4 °C. Between each centrifugation, the pellet was discarded, and the supernatant was collected subjected to further centrifugation. The supernatant was then filtered (size 0.45 µm) through a vacuum filter and was subjected to centrifugation at 10 000 x g for 1 h[7]. The resulting solution was again filtered through a vacuum filter using a 0.22 µm filter paper. The samples were collected and refrigerated at −80 °C for lyophilization (Freezone 12 Freeze drier, Labconco, Kansas City, USA). Lyophilisation, also known as freeze drying, removes water from the liquid PDEVs by reducing the pressure to allow the frozen water to sublimate. This is done by freezing the samples and then placing it in the lyophilizer which is left for 16 h to dry. The lyophilised samples were then stored at −80 °C for further application and characterisation.

Preparation of itraconazole-loaded PDEVs

Itraconazole (10 mg) was dissolved in 2 mL dichloromethane (DCM) and added to the PDEVs (250 mg) dissolved in distilled water (98 mL) and mixed. The samples were left at room temperature for 10 min and then sonicated (Sonics Vibra Cell, Newtown, CT, USA) for 2 min x 5 cycles (pulse: 5 s on, 2 s off), 40% amplitude[25]. The samples were left to rest for 10 min between each cycle. After sonication, the samples were incubated for 1 h at 37 °C and left at 4 °C overnight[26,27]. The next day, the samples were centrifuged at 12 500 x g for 90 min, and the pellet was recovered and stored in PBS (pH = 7.4) at −80 °C. The supernatant was retrieved for quantification of entrapment efficiency.

Profiling and characterisation of extracted PDEVs

Protein determination by the bicinchoninic acid assay (BCA) assay

Protein contents were measured using a BCA protein assay kit (Thermo Scientific Pierce, Rockford, IL, USA). BSA standard (25 µL) were transferred to a 96 well plate to which 200 µL working reagent was added (working reagent 50:1 ratio of assay reagents A and B). The plate was incubated for 30 min at 37 °C, before being analyzed with a spectrophotometer at 562 nm using Victor™ X3 microplate reader. A calibration curve was drawn using the BSA standard readings. The PDEVs were dissolved in PBS (pH = 7.4) (1 mg/mL). 25 µL of the PDEVs samples were mixed with 200 µL of the working reagent which was then read on the spectrophotometer at 562 nm. The protein content was quantified using the calibration curve as stipulated above.

Size and zeta potential determination of PDEVs

The freeze-dried PDEVs and drug loaded PDEVs were used to measure zeta potential, average particle size, and polydispersity index (PDI) using Malvern ZetaSizer Nano ZS (Malvern Instruments, Worcestershire, UK).

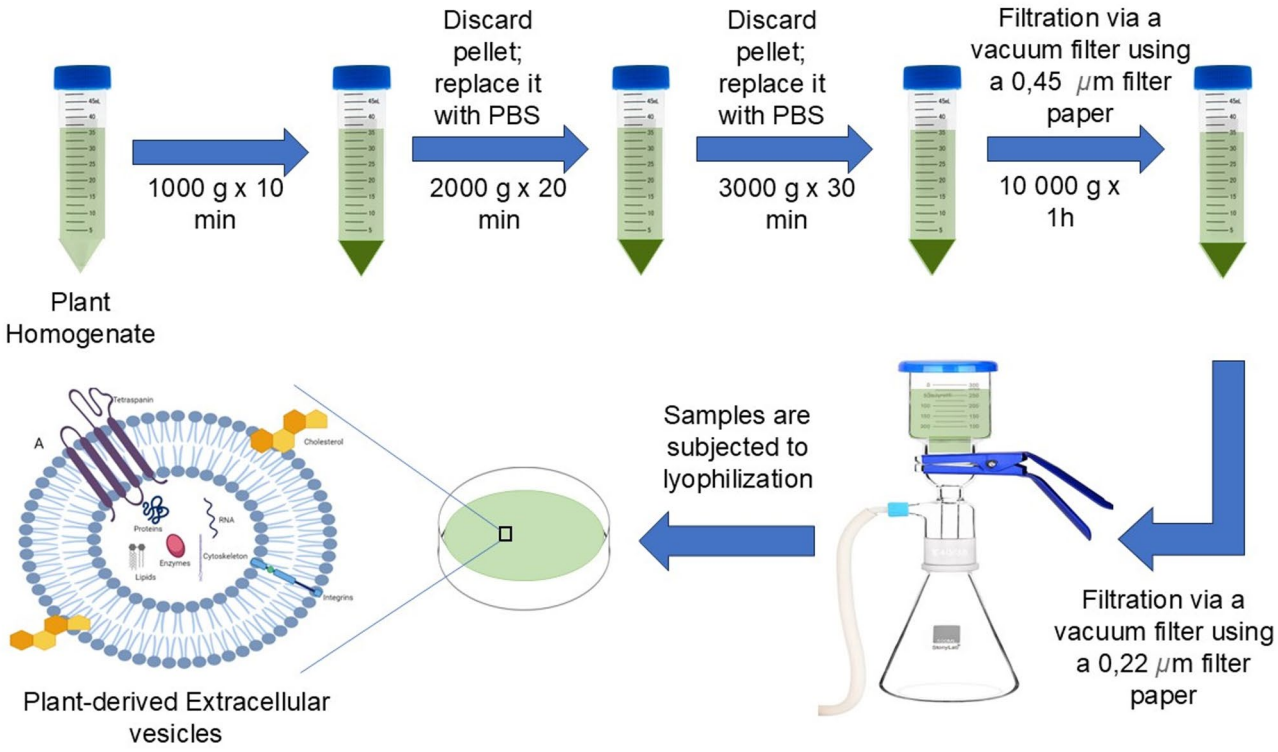

Fig. 1. Extraction procedure of plant derived extracellular vesicles, Preparation and characterization of loaded PDEVs.

Samples were prepared with distilled water to a final concentration of 1 mg/mL, and about 2 mL of the samples were placed in the cuvette and measured. All the measurements were carried out in triplicate and analysed using Zetasizer Nano ZS Software[28].

Surface morphology of PDEVs

The morphological examination of the PDEVs and the drug loaded PDEVs were analysed by scanning electron microscopy (SEM) (Zeiss Electron Microscopy, SIGMA VP, Carl Zeiss Microscopy Ltd, Cambridge, UK)[29]. The lyophilized samples were dissolved in PBS (pH = 7.4), and a drop was positioned on an aluminium specimen stub and left overnight to dry. Subsequently, the samples loaded on the stub were sputter-coated with gold. The SEM pictures of the samples were generated with the help of SEM using the Zeiss Imaging Software.

Determination of ITZ entrapment efficiency and loading capacity within the PDEVs

The entrapment efficiency (EE) of ITZ within the PDEVs were evaluated using both the direct and indirect method. The indirect method includes using the supernatant collected after drug loading which was analysed using the High-performance liquid Chromatography (HPLC) quantification technique outlined below. The EE was calculated using Eq. 1. The direct method involved rupturing the pellet using sonication to release the drug which was then quantified using HPLC. The EE was calculated using Eq. 2[30]. The concentration was computed using a standard linear curve of ITZ (R^2 = 0.9991). The drug loading capacity (DLC) refers to the maximum amount of drug that can be incorporated into a delivery system calculated using Eq. 3[31].The percentage value of EE of the drug loaded PDEVs were carried out in triplicate (n = 3) and calculated using the equations below:

$$Entrapment\ efficiency\ (\%) = \frac{Initial\ Concentration\ of\ drug - Free\ drug\ concentration\ in\ Supernatant}{Initial\ Concentration\ of\ drug} \times 100 \quad (1)$$

$$Entrapment\ efficiency\ (\%) = \frac{Drug\ concentration\ in\ pellet}{Initial\ Concentration\ of\ drug} \times 100 \quad (2)$$

$$Drug\ Loading\ Capacity = \frac{total\ amount\ of\ drug\ in\ PDEVs}{total\ amount\ of\ PDEVs} \times 100 \quad (3)$$

Quantification of Itraconazole from the PDEVs using high-performance liquid chromatography

Quantification of ITZ was performed using high-performance liquid chromatography (HPLC) (Waters, Milford, MA, USA)[32]. Isocratic method was carried out using XSelect™ CSH C18 (dimensions: 250 mm x 4.6 mm, pore size: 5 µm) column. The mobile phase used was acetonitrile, and a combination of 0.1% Triethylamine and 10% methanol at a ratio 90:10 at a flow rate of 1.8 mL/min, injection volume was 10 µL, column was at room temperature and itraconazole was detected at 265 nm using an ultraviolet (UV)-visible detector[33]. Itraconazole had a retention time of 2.2 min, and the overall run time was 5 min.

Evaluation of the chemical composition of ITZ-loaded PDEVs

Pure ITZ, blank PDEVs, and loaded PDEVs were analysed in powdered form (obtained by lyophilisation) to determine the chemical composition of the drug and the PDEVs. The formulations were analysed in triplicates (n = 3) with Spectrum 2000 ATR-FTIR (Perkinelmer, Beaconsfield, BUCKS, UK)) with the wavelength ranging between 4000 and 650 cm^{-1} with the spectra recorded as an average of 20 scans[34]. A background scan was performed before each measurement to eliminate noise.

In vitro analysis of ITZ release from the PDEVs

In vitro release studies were done on drug loaded PDEVs to determine ITZ release behaviour using the dialysis method[35]. Itraconazole loaded aloe, ginger and BCS PDEVs were added (~ 7–8 mg of ITZ in the loaded PDEVs dispersed in 5 mL of PBS (pH = 7.4)) into the dialysis tubing and immersed in 95 mL release medium separately. The tubing was placed in vessels containing PBS at pH 7.4 and pH 6 (containing 0.5% SLS to allow wetting and dissolution of drug) and incubated at 37 °C in a horizontal orbital shaking incubator (type LM-530, Yihder Technology Co., Ltd., New Taipei City, Taiwan), set at 25 rpm. The selected pH at 7.4 and 6 is to mimic the brain extracellular fluid and the tumour environment respectively. Sampling was conducted at stipulated periods; 1 h, 2 h, 4 h, 6 h, 8 h, 12 h, 24 h, 48 h, 72 h, 96 h and thereafter weekly for 20 days. All aliquots were run through HPLC using the method outline above. The experiments were conducted in triplicate (n = 3) on all the formulated loaded PDEVs in both pHs.

To analyse the in vitro drug release data, various kinetic models such as zero-order, first-order, Higuchi, Korsmeyer-Peppa, and Weibull release model were used to determine the release kinetics[36,37]. All the equations are provided in the supplementary material.

Cytotoxicity and cellular internalization studies

Cell culture of A172 and HaCaT cells

A glioblastoma A172 and HaCaT keratinocytes cell line (obtained from ATCC, USA) were each cultured in DMEM, supplemented with 10% FBS and 1% penicillin-streptomycin. The cells were incubated under 5% CO_2 at 37 °C in an incubator. Cells were sub-cultured upon reaching 80–90% confluency using 0.25% trypsin and only cells between passages 26 and 28 were used for experiments to ensure consistency and viability. All the experiments were done in triplicates (n = 3).

Assessment of cytotoxicity of the PDEVs

A172 cells were seeded in a 96-well plate at a density of 3000 cells/well and HaCaT cells were seeded in a 96-well plate at a density of 7500 cells/well and allowed to incubate overnight. Thereafter, the cells were treated with various concentrations of blank PDEVs (0.25–4 mg/mL), loaded PDEVs (0.625–0.039 mg/mL) and pure drug (500–31.25 µM). A positive control – cell culture medium with no treatment, and negative control – cell culture medium with 10% DMSO were added for each plate. After 24, 48, and 72 h 3-(4, 5-methylthiazol-2-yl)−2, 5-diphenyl-tetrazolium bromide (MTT, Sigma-Aldrich) was added (10 µL/well) for 4 h and formazan crystals were solubilized by the addition of Sodium Dodecyl Sulphate (SDS). The plates were read at 570 nm using Victor™ X3 microplate reader. % cell viability was calculated using the equation below:

$$\%\, Cell\ Viability\ :\ \frac{Absorbance\ of\ Treatment}{Absorbance\ of\ Negative\ Control}\ \times\ 100 \tag{4}$$

Evaluation of cell uptake and internalization

Fluorescein isothiocyanate (FITC) was used as a dye to label ITZ loaded PDEVs[38]. Briefly, FITC (1 mg) was dissolved in 1 mL of DMSO (1 mg/mL), 100 µL of the solution was added to 200 µg of loaded PDEVs. The solution was incubated for two hours and centrifuged at 14,000 rpm for 20 min (TC-MiniSpin Centrifuge, TopScien, Ningbo, China). The recovered pellet was washed with distilled water to remove unbound FITC. The FITC-labelled PDEVs were collected and used immediately.

The A172 cells were cultured as described previously and employed for the uptake study. Cells were seeded (1×10^5 cells/well) on presterilized cover slips in a 6-well plate and incubated for 24 h at 37 °C and 5% CO_2. After incubation, the cells were treated with FITC-labelled PDEVs and further incubated for 24 h, while control cells were not treated. After 24 h, all wells were spiked with 500 µL of 4% paraformaldehyde (PFA) for 2 min to condition the cells to the fixation solution. Thereafter, the media was removed, and cells were fixed with 2 mL of 4% PFA for 20 min. The cells were washed three times with 2mL of PBS (pH = 7.4) and stained with DAPI (1 ug/mL), followed by incubation for 5 min in the dark at room temperature[39]. The cover slips were then used under a fluorescent microscope (Celena S Microscope, Logos Biosystems) to view and capture images of the cell at 517 nm green, fluorescent excitation (FITC) and 461 nm blue fluorescence excitation (DAPI) using the 10X objective lens[40].

Determination of BBB permeability of the ITZ-loaded PDEVs

A Bioassay™ PMBBB method (Hayward, CA, USA) was used to determine the permeability of compounds. The PMBBB, which consists of porcine brain lipid extract dissolved in dodecane, was optimized to predict BBB passive permeability. This membrane was immobilized on a PVDF matrix of a 96 well "acceptor" filter plate placed on top of a 96 well "donor" plate. The test controls, stocked in 10 mM DMSO solutions, and the samples were diluted to 500µM aqueous phosphate buffer and the concentration of DMSO was 0.5% in the final solution according to the protocol. The test controls and samples were added to the donor plate and placed in the acceptor plate containing 300 µL of PBS (pH = 7.4). The plate was then placed in the incubator at 37 °C for 18 h. The acceptor solution was then tested using a Victor™ X3 microplate reader compared to its standards. Permeability Rate (Pe) calculations were performed using the equation below and were expressed in units of cm/s.

$$P_e = C\ \times\ -lnln\,(1 - \frac{OD_A}{OD_E}) \tag{5}$$

Where OD_A is the absorbance of Acceptor Solution minus Blank, OD_E is the absorbance of the Equilibrium Standard minus Blank, and, using an 18-hour incubation, C = 7.72×10^{-6} as provided in the manufacturer's protocol.

Statistical analysis

All data were expressed as mean values ± standard deviation.

Results and discussion

Isolation and characterization of the PDEVs

Aloe, ginger and black cumin seeds (BCS) were selected to investigate their potential of drug encapsulation and their ability to permeate the BBB. These plants were selected for their clinical properties. PDEVs were extracted via serial centrifugation and double filtration from the different plant sources. The mean particle size, PDI and zeta potential are critical parameters of drug delivery systems for cellular uptake and internalization, bioavailability, stability and effective clinical applications[41]. After isolation of PDEVs, their particle size distribution ranged from 50 to 150 nm, with a mean size of 130 ± 2.79 nm for aloe, 103.5 ± 1.09 nm for ginger and 141.4 ± 1.15 nm for BCS (Fig. 2D). For effective BBB permeation, size is a critical parameter which needs to be < 200 nm[42]. Therefore, the size of the isolated PDEVs meet this criterion and may prove advantageous for crossing the BBB. The PDI value < 3.0 indicates homogeneity and stability of the PDEVs (Table 1)[41]. The homogeneity of PDEVs ensures optimal cellular uptake and equal biodistribution of PDEVs[41].

The presence and morphology of PDEVs were confirmed by Scanning Electron Microscopy (SEM) (Fig. 2A-C). The SEM analysis showed that there were numerous PDEVs with a spherical morphology and distributed unevenly throughout the surface. These PDEVs had a range of dimensions with diameter around 100 nm or less. The SEM confirms that the PDEVs extracted are nano-sized vesicles with a spherical morphological shape. This also validates the isolation technique as it allows the PDEVs to retain their round shape[20].

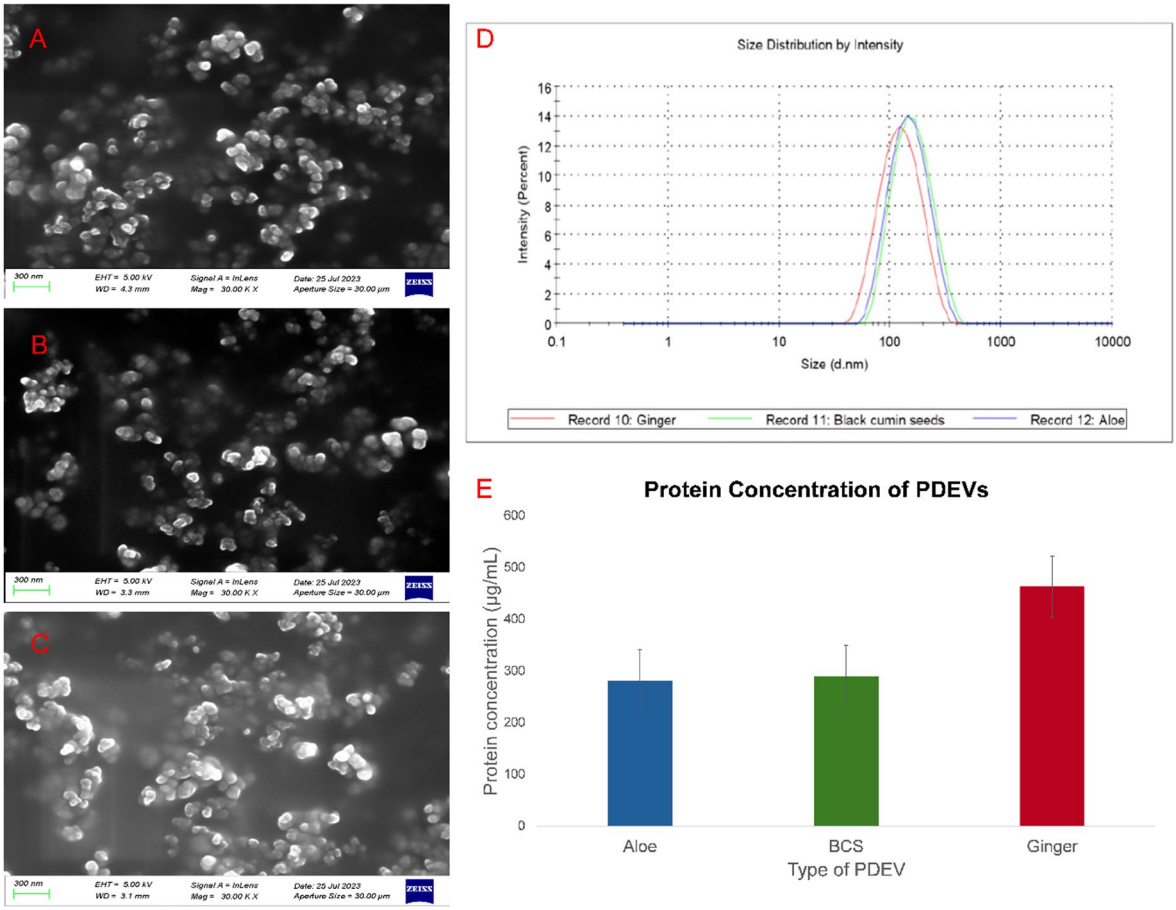

Fig. 2. Size distribution, morphology and protein concentration of the blank PDEVs: (**A**) SEM image of Aloe EVs; (**B**) SEM image of Black cumin seeds EVs; (**C**) SEM image of Ginger EVs; (**D**) Dynamic light scattering (DLS) size measurement of blank PDEVs and (**E**) Protein Concentration of PDEVs.

Plant type for EV derivatization	Average size(nm)	PDI	Zeta potential(mV)
Aloe	130 ± 2.79	0.196 ± 0.008	−18.1 ± 0.44
Ginger	103.5 ± 1.09	0.213 ± 0.003	−17.3 ± 0.32
Black cumin seeds	141.4 ± 1.15	0.179 ± 0.004	−11.2 ± 0.68

Table 1. Average size, PDI and zeta potential of blank PDEVs.

The zeta potential of the PDEVs ranged from − 11 to −19 mV for the different PDEVs (Table 1). These results align with reported literature where a higher negative zeta potential (−10 to −30 mV) was shown to prevent aggregation and provide stability to the system, while also avoiding rapid clearance by the immune system[43]. BCS has the lowest anionic zeta potential which suggests it may have a lower stability compared to aloe and ginger EVs. The BBB itself is highly negatively charged making it difficult for highly negatively charged particles to penetrate through. However, negatively charged particles have lower cytotoxicity and low macrophage uptake leading to a higher circulation time in the body[44]. A study highlighted that cationic nanoparticles exert a toxic effect on the BBB and disrupt its integrity whereas neutral or low concentrations of anionic nanoparticles had no such effects on the BBB integrity[42].

Protein assays of the PDEVs were performed using a BCA protein Assay kit and the protein content was found to be 282.15 ± 65.47, 290.62 ± 20.16, and 463.70 ± 79.15 µg/mL in 1 mg/mL concentration of aloe, BCS, and ginger EVs respectively (Fig. 2E). All different PDEVs had different amounts of protein levels which may correlate to cytosolic or enzyme proteins[12]. Some of these enzymes may be beneficial and some may produce unwanted interactions. Hence serial centrifugation is important to remove most of the unknown protein content, however some of the proteins may remain preserved due to the lyophilisation process[45] (Fig. 2E).

The FTIR spectra of extracellular vesicles derived from BCS, ginger, and aloe revealed distinct biochemical compositions. In the 3200–3400 cm^{-1} region, PDEVs exhibited an intense broad peak, indicating the presence of hydroxyl and amine groups. The lipid-associated C-H stretching peaks (2800–2950 cm^{-1}) are also observed

for the PDEVs. BCS has been proven to have a high lipid content, in a study by Albakry et al., which further supported the obtained results[46]. Protein-related amide I (1600–1700 cm^{-1}) and amide II (1500–1570 cm^{-1}) belonging to the carbonyl (C = O) stretch, showed peaks for all PDEVs. The protein content directly correlates to the BCA results in this study shown in Fig. 2. The peaks observed at 1000–1250 cm^{-1}, correlates to C-N stretching vibrations which are indicative of biomolecules and peptides which possess the amine functional group.

In contrast, the fingerprint region (1000–500 cm^{-1}), associated with carbohydrates and phosphates suggests carbohydrate content in all the PDEVs. Aloe plant extract contains more than 75 different compounds, some of which includes sugars (monosaccharides such as mannose-6-phosphate and polysaccharides such as glucomannans), anthraquinones (aloin and emodin), fatty acids (i.e., lupeol and campesterol) and many others[47]. The FTIR depicts similar chemical composition of the aloe EVs in Fig. 3 with carbohydrate and lipid content. *Nigella sativa seeds* (BCS) are rich in unsaturated and essential fatty acids suggested by many studies with potential alkaloids such as isoquinolone promoting anticancer effects[48]. The lipid content of BCS and ginger may make it easier to cross the BBB because of its lipophilicity. The chemical composition may affect the drug loading capacity and release behaviour of the three PDEVs.

Drug loading and characterisation of Itraconazole loaded plant-derived extracellular vesicles

Aloe, Ginger and BCS- derived EVs were loaded with Itraconazole (ITZ) to assess entrapment efficiency and drug loading capacity. A combination method of sonication and incubation was employed. Sonication provides a high-efficient method for drug encapsulation in EVs, however EVs are susceptible to membrane damage while the incubation method affords low drug encapsulation but a high rate of membrane recovery[49]. During sonication, transient pores of integrity of the membrane of the PDEVs allows diffusion of substances from the surrounding medium[50]. Inspired by this, we proposed a method which combines both sonication and incubation

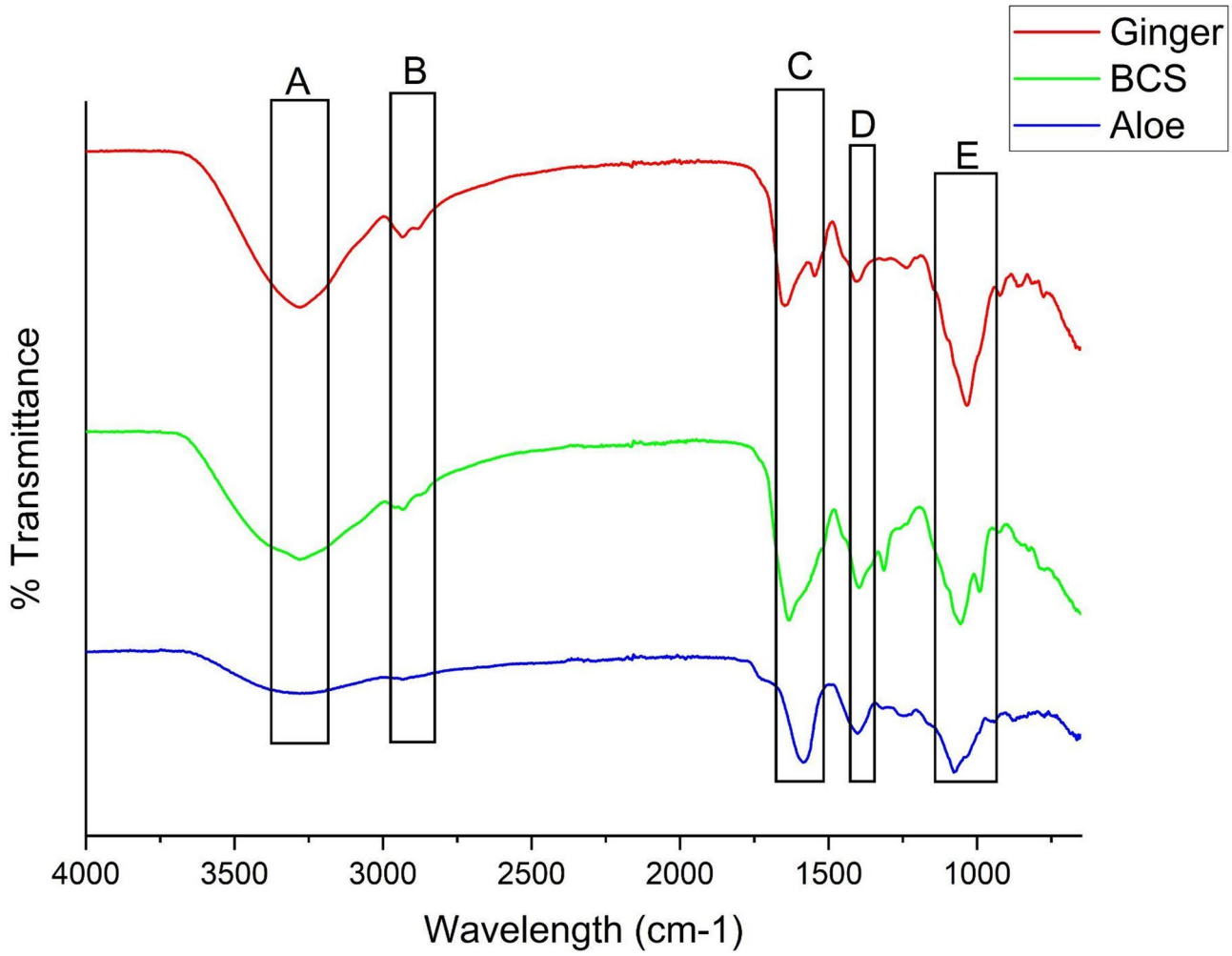

Fig. 3. FTIR spectra to analyse the chemical composition of PDEVs. Characteristic bands of lipids, proteins and carbohydrates are highlighted in the plots. (**A**) highlight the hydroxyl and amine groups between 3200–3400 cm^{-1}, (**B**) indicate lipid-associated C-H stretching between 2800–2950 cm^{-1}, (**C**) and (**D**) indicate the protein region at 1600–1500 cm^{-1} and (**E**) 1000–1200 cm^{-1} highlights the C-N stretches of the compound.

Plant type EVs	Average size (nm)	PDI	Zeta potential (mV)	%EE	%DLC
ITZ loaded Aloe	290.4 ± 5.71	0.236 ± 0.0127	−14 ± 0.44	82.09 ± 2.38	3.2 ± 0.094
ITZ loaded ginger	179.3 ± 3.00	0.132 ± 0.0216	−13.6 ± 0.173	83.05 ± 6.54	3.2 ± 0.28
ITZ loaded black cumin seeds	415.8 ± 7.09	0.553 ± 0.070	−10.5 ± 0.68	72.80 ± 3.59	2.8 ± 0.20

Table 2. Average size, PDI, zeta potential, % EE and % DLC of Itraconazole loaded plant-derived EVs.

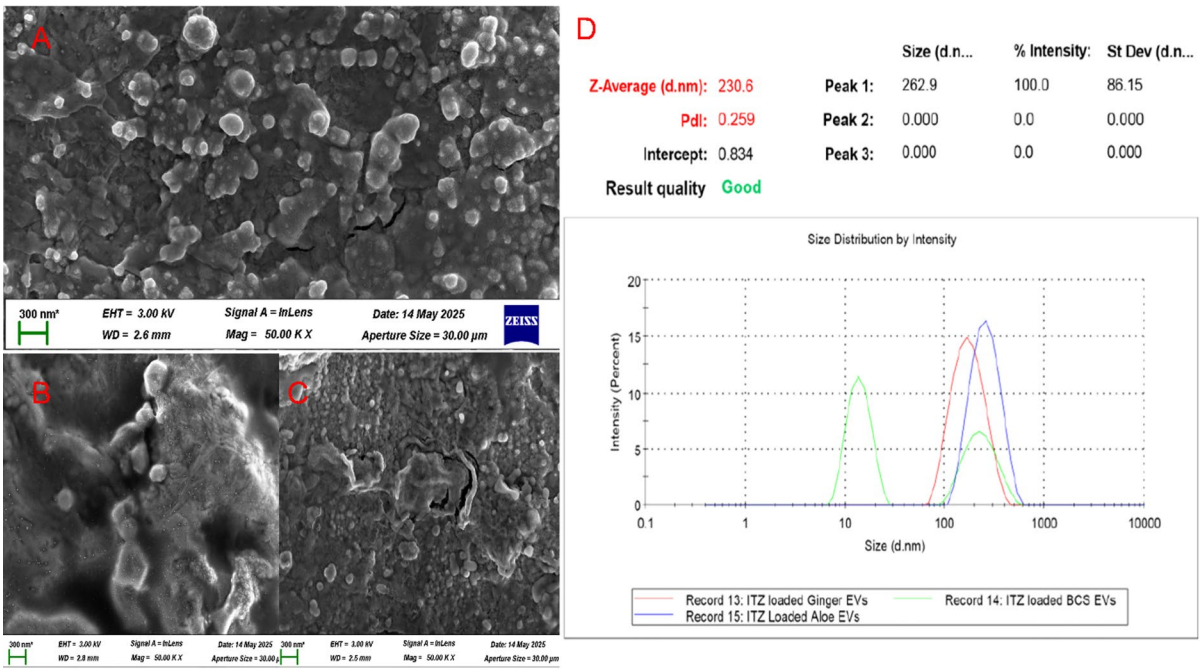

Fig. 4. Size and morphology of loaded PDEVs: (**A**) SEM of ITZ loaded Aloe EVs; (**B**) SEM of ITZ loaded BCS EVs; (**C**) SEM of ITZ loaded Ginger EVs and (**D**) Size distribution map of all loaded PDEVs.

with the help of the evaporative behaviour of DCM to enhance drug loading. Moreover, to prevent drug leakage; a 10-minute rest between each cycle of sonication was added and sonication was done with an on and off pulse function to avoid excessive sonication. The size distribution of the aloe, ginger and BCS loaded EVs increased to 290.4 ± 5.71, 179.3 ± 3.00 and 415.8 ± 7.09 nm respectively suggesting successful drug encapsulation (Table 2). The PDI in Table 2 shows that the drug-loaded ginger EVs have the best uniform dispersion with a PDI of 0.132 ± 0.0216 suggesting the equal distribution of drug inside the PDEVs resulting in a size of 179.3 ± 3.00 nm[41]. However, the increased size of aloe and BCS is high which may also be due to the vesicles being aggregated resulting in less PDEVs loaded with more drug. BCS loaded PDEVs size is the largest which may be due to the high lipid content able to attract more lipophilic drug ITZ. The size distribution map of BCS in Fig. 4D shows how most of the BCS EVs remained unloaded which may be because of the high lipid content on the membrane of the BCS EVs making them more rigid and stable hence making it difficult to break open[51]. This can also be noticed by the lower entrapment efficiency of the BCS EVs (Table 2).

The morphology of the loaded PDEVs can be seen in Fig. 4(A-C), with loaded aloe EVs having a rounder morphological shape compared to the other two PDEVs. It is evident through Fig. 4B that BCS EVs do not retain their morphological shape which may be due to the extraction or drug loading technique. The zeta potential of the PDEVs increased and the conductivity became less anionic, increasing the potential of cell permeability as stated above that cell membranes are negatively charged (Table 2)[44].

The entrapment efficiency of the PDEVs was between 72 and 85% for all the PDEVs, the EE did not vary significantly amongst the PDEVs. The drug loading capacity is 2.8–3.2% compared to the total component of the delivery system indicating moderate DLC. The PDEVs loaded formulation was optimised by varying the PDEVs and drug feeding ratios. The amount of itraconazole was increased to a constant quantity of aloe EVs by different feeding ratios i.e. 5:250, 10:250, 15:250 (mg of drug: mg of EVs). The EE did not increase significantly with the increasing amount of drug, however the DLC increased up to 4% suggesting that more quantity of drug can be loaded in the same amount of PDEVs which indicates that there are more PDEVs in the system that can accommodate higher amounts of drug. Numerous studies have reported that EVs typically demonstrate modest drug loading due to their intrinsic membrane capacity, and our values fall within the commonly published range[5,25,35,52].

FTIR spectroscopy was employed to assess the successful encapsulation of the drug within the PDEVs. Spectra were obtained for the blank drug (Pure ITZ), blank PDEVs, and the loaded PDEVs, and the results are presented in Fig. 5. The spectrum of the blank PDEVs displayed characteristic absorption bands around 3300 cm^{-1} corresponding to O-H/N-H stretching vibrations, and bands near 1650 cm^{-1} and 1540 cm^{-1} indicative of amide I and amide II carbonyl (C = O) stretch, respectively. In contrast, ITZ showed several distinct peaks in the region (1000–1700 cm^{-1}), characteristic of its specific functional groups in the free crystalline state. Upon drug loading, the spectrum exhibited shifts and changes in intensity, particularly in the regions corresponding to the amide bands and the broad O-H/N-H stretch. Additionally, the region (1000–1700 cm^{-1}) of the loaded PDEVs showed significant attenuation and broadening of the EV's peaks, suggesting a possible interaction between the drug and the vesicle matrix or changes in blank PDEV structure. The reduction in sharpness and intensity of ITZ specific peaks and the visibility of the PDEV specific peaks in the loaded aloe EVs hence no observable new characteristic peaks were found in the FTIR spectra. Therefore, it could be predicted that no chemical reaction might have occurred in the process of encapsulation in the PDEVs. The interactions that occur may be due to non-covalent interactions[53,54].

In vitro drug release of ITZ from PDEVs

All the drug release studies were conducted under sink conditions to ensure precision of the results[55]. The drug release studies were carried out using the dialysis bag method at 37 °C. Hence, the solubilities of the drug in different release mediums were determined prior to the release study. The selection of release medium was based on an optimum solubility of ITZ and no interaction with the PDEVs. The release medium was 0.5% SLS in PBS (pH = 6.0 and 7.4). The samples were collected at various timepoints and quantified using HPLC. The release profiles of ITZ loaded PDEVs are plotted in Fig. 6 with cumulative release percentage plotted along the Y-axis and the time (hours) along the X-axis. The drug release profile of all the PDEVs was less than 50% of releasing over a period of 21 days. The aloe EVs had a 16 ± 0.71% ad 20 ± 2.14% IZ release at pH 7.4 and 6.0, respectively. The release had an initial burst of 4.45 ± 2.15 and 10.47 ± 2.42% a pH 7.4 and 6.0 respectively within 24 h and the remaining curve shows a controlled release profile over 504 h. This was not seen with BCS EVs as it had a higher release at both pH i.e. 21 ± 1.01% ad 32 ± 8.87% rlease at pH 7.4 and 6.0 respectively. BCS EVs had a higher release within 24 h which is 10.27 ± 0.44% a pH 7.4 and 11.27 ± 2.28 at pH 6.0. Cumulative release from

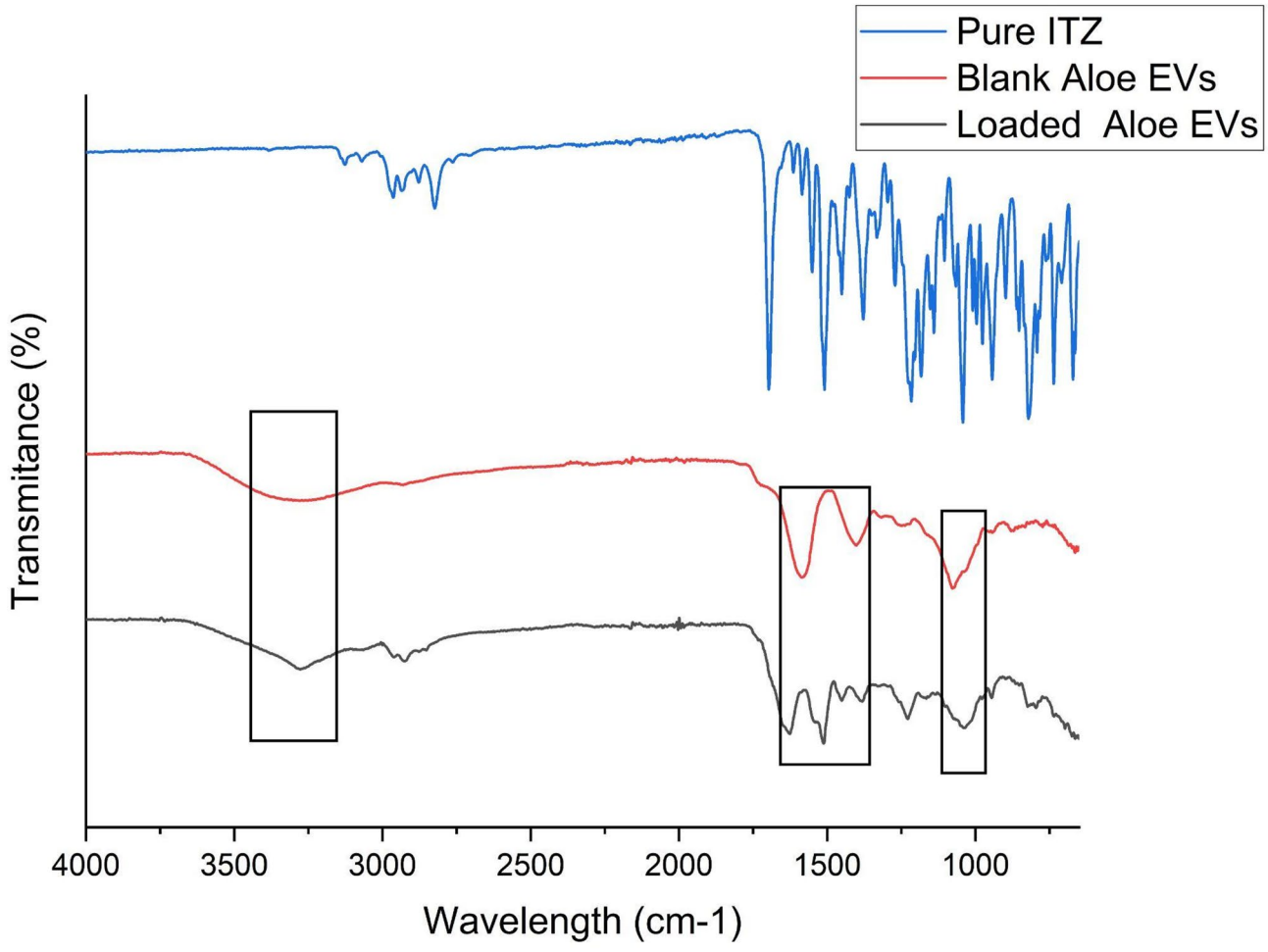

Fig. 5. FTIR spectra of blank aloe EVs (Red), Pure Itraconazole drug (Blue) and Loaded aloe EVs (Black).

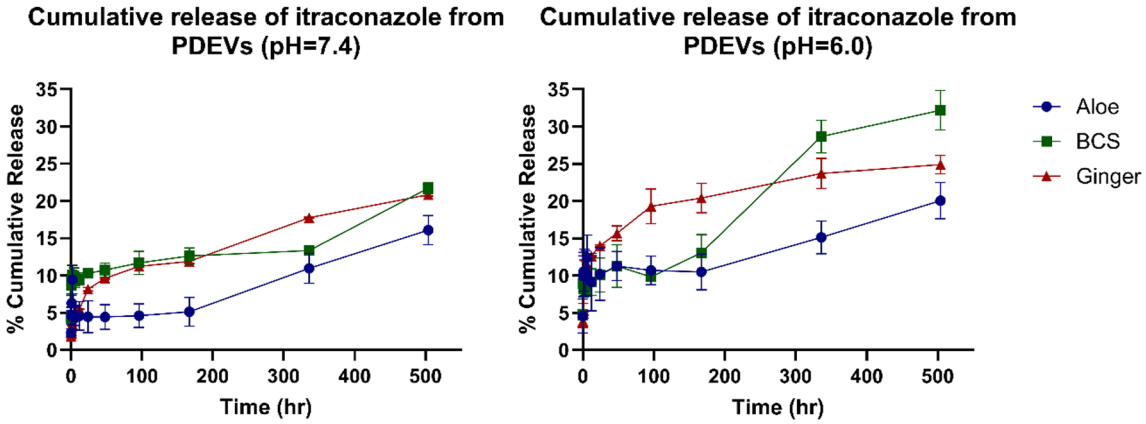

Fig. 6. Cumulative release (%) of itraconazole from aloe, BCS and ginger PDEVs at pH 7.4 and 6.0.

ginger EVs was 20 ± 1.03% ad 24 ± 0.43% a pH 7.4 and 6.0 respectively Within 24 h, ginger EVs had a lower release which was 8.14 ± 0.23% a pH 7.4 and 13.99 ± 0.12% a pH 60. It appears that BCS had the highest release which may be due to its higher zeta potential. Passive drug release from EVs can be affected by the size, shape, zeta potential and the composition of the EVs[43]. Proven above, the size of BCS increased to 415.8 nm (Table 2) which contributes to the higher % of drug release as more drug could have been released in lesser quantities of BSC EVs. However, with aloe and ginger due to its relatively smaller size and rounder morphological shape, it might have prolonged the release of the drug from different PDEVs due to a higher surface area[56]. The irregular encapsulation of BCS EVs also contributes to the irregular release profile as seen in Fig. 5 whilst ginger and aloe provide more controlled release over time. The composition of the EVs may also affect the drug release profile. The observed increase in passive drug release of BCS may be due to the lipid composition which may be enriched with unsaturated fatty acids, as inferred from the known lipid profile of Nigella Sativa plant[46]. Such composition promotes higher membrane fluidity due to the surrounding release medium. Furthermore, it is important to note that the in vitro release test primarily reflects passive diffusion of ITZ from the PDEVs through the dialysis membrane. In vivo, additional processes such as enzymatic membrane degradation, serum interaction, cellular uptake and endosomal escape would further contribute to drug release[20]. Therefore, the limited release observed in vitro likely represents a conservative estimation of the drug that would be liberated under physiological conditions.

The slow controlled release of ITZ can be leveraged for a sustained drug delivery system. Sustained-release drug delivery systems achieve the slow release of a drug over an extended period after administration of a single dose. These delivery systems include implants, skin patches, inserts etc. which are convenient to patients and need a sustained drug release system[57]. Further use of these PDEVs as part of a drug delivery system with sustained release is to manage recurrence of GBM. GBM is the one of the most aggressive tumours and recurrence is almost unavoidable which is due to the poor prognosis and no standard care in clinical situations[58]. In this regard, different approaches need to be investigated, in which PDEVs are a potential for sustained release of drug to manage recurrence of GBM over time.

The observed pH-dependent release profile with enhanced drug release under a pH of 6.0 may be attributed to the acidic medium making the PDEV membrane weaker. At lower pH, increased protonation of lipid head groups likely reduces membrane integrity, promoting faster drug diffusion. In contrast, at higher pH, deprotonation enhances lipid packing and membrane stability, thereby slowing the release rate[59]. This effect takes place through stimuli-responsive release of the drug from the PDEVs hence proving the mechanism may be similar to synthetic nanoparticles such as liposomes[60]. The pH-triggered drug release is advantageous to deliver drugs to tumour sites which are typically at low pH (6.5–6.8)[61,62].

For the drug release kinetic study, different mathematical models were used namely Korsmeyers-Peppa, Higuchi, First-order, Zero-order and Weibull release model comparing the R-square values and rate constants from the plots of the models (provided as supplementary material)[36,37]. The zero-order rate explains the systems where the rate of drug release does not depend on its concentration. The first order explains the release from the system where rate of drug release is concentration dependent. Higuchi described the release of drugs from an insoluble matrix as a square root of time dependent process based on Fickian diffusion. Korsmeyer-Peppa model derives a simple mathematical relationship describing the drug release from different polymeric systems. The Weibull release model is an empirical model widely used for both immediate and sustained drug-release patterns[36,37].

In the table above, R^2 is the correlation value, K is rate constant, and n is the release exponent (Table 3). Based on best fit with the highest correlation value, it is concluded that Aloe and BCS loaded EVs follow the zero-order model at both pH (7.4 and 6.0) and ginger loaded EVs follow the Korsmeyers-Peppa and the Weibull model. Zero-order model describes the release process where the drug is released at a constant rate over time, regardless of its concentration. Aloe and BCS loaded EVs release the drug at a constant rate which is ideal for maintaining steady drug levels in the body. The Korsmeyer-Peppas model is useful when the release mechanism involves a combination of processes which may be the case with ginger loaded EVs as it also follows the Weibull model of

Sample		Higuchi	Korsmeyers	First-order	Zero-order	Weibull
Aloe (pH = 7.4)	R^2	0.551	0.3091	0.5787	0.7219	0.3093
	K	0.0498	0.0264789	0.00004606	0.0003	-
	n	-	0.1111	-	-	-
Aloe (pH = 6.0)	R^2	0.6421	0.5117	0.4922	0.7149	0.5143
	K	0.0507	0.0569246	0.00002303	0.0003	-
	n	-	0.0943	-	-	-
BCS (pH = 7.4)	R^2	0.7708	0.6947	0.5905	0.8001	0.6953
	K	0.0617	0.04728245	0.00002303	0.0004	-
	n	-	0.1173	-	-	-
BCS (pH = 6.0)	R^2	0.8598	0.7103	0.8547	0.9397	0.6998
	K	0.1371	0.03397035	0.00004606	0.0008	-
	n	-	0.1739	-	-	-
Ginger (pH = 7.4)	R^2	0.9756	0.9865	0.5943	0.8715	0.9866
	K	0.1079	0.00689763	0.00006909	0.0006	-
	n	-	0.3258	-	-	-
Ginger (pH = 6.0)	R^2	0.8594	0.9217	0.4416	0.672	0.929
	K	0.1158	0.02435006	0.00004606	0.0006	-
	n	-	0.2369	-	-	-

Table 3. Mathematical modelling of Itraconazole release kinetics from plant-derived extracellular vesicles: interpretation of R-square values and rate constants.

kinetics. The Weibull model is applicable when the release is from heterogeneous matrices. Other parameters of the Weibull model include β which relates to the release mechanism of the ginger loaded EVs. β of 0.3383 (pH = 7.4) and 0.2525 (pH = 6.0) indicates a diffusion-controlled release which may be in combination with other processes which are unknown[63]. The n value predicts the release mechanism of the drug which is less than 0.45 corresponds to the Fickian diffusion model[37]. Fickian diffusion is controlled purely by diffusion due to a concentration gradient, and the rate of drug release slows down over time as the gradient diminishes.

Cytotoxicity assessment of the PDEVs, ITZ and the loaded PDEVs

To provide insight into the potential application of PDEVs for therapeutic applications, it is essential to confirm the cytotoxicity of the drug delivery system. As shown in Fig. 7, the cytotoxicity profile of PDEVs is determined in A172 and HaCat cells to compare the treatments in both cancerous and non-cancerous cell lines using an MTT assay. Both cells were treated with the same concentrations of PDEVs for 24, 48 and 72 h. In A172 cell line, the aloe PDEVs shows increased cell viability at both low and high concentrations, the lowest cell viability is 74% at 24 h in A172 cell line. However, the cell viability has not changed significantly at different timepoints. The cell viability of aloe EVs in HaCat cells is higher compared to the A172 cells in correlation with the concentration. The proliferative effects of aloe PDEVs are seen through its enhanced cell viability on the HaCat cell line however it seemed to inhibit proliferation of A172 cell lines. This proves that aloe EVs may possess the characteristics of the plant which have been proven to have characteristics such as anti-cancer activity and proliferative activity on normal cells[64,65]. The loaded aloe EVs have a lower cell viability compared to the blank aloe EVs despite the lower concentration in both cell lines. This might be due to the release of itraconazole during cellular uptake as the mechanism of uptake is yet unknown. *Nigella Sativa* has been reported as cytotoxic at higher concentrations in many studies, as shown in Fig. 6 both blank and loaded BCS EVs have a higher cytotoxicity even at low concentrations[66]. This is seen in both A172 and HaCat cell lines however at 0.25 mg/ml, it can be deduced that BCS EVs may have some proliferative activity on HaCat cell lines and anti-cancer activity on A172 cell line resulting in 81% and 117% cell viability at 72 h respectively. With the loaded BCS EVs, having a lower cell viability even at lower concentrations which may be due to the release of ITZ. The cell viability of loaded BCS EVs reasonably correlates to the cell viability of pure ITZ in Fig. 8 further proving the release of the drug from the BCS EVs affecting the cell viability of both cell lines. BCS contains thymoquinone which has been reported to induce apoptosis in various cancerous cells further supporting its effects on the A172 cell lines compared to the HaCat cell line[67].

Cytotoxicity of ginger EVs and ITZ loaded ginger EVs against A172 and HaCat cell lines has been displayed in Fig. 7. Blank ginger EVs display strong cytotoxic effects towards both cell lines at higher concentrations with the lowest activity in HaCat cell lines. Blank ginger EVs showed more toxic effects against A172 cell line than the anti-cancerous cell line at concentrations lower than 0.50 mg/ml. It is well known and proved by many studies that ginger possesses anti-cancer activity and has been shown to suppress tumours of many cancers[68,69]. In this research, it has been proven that EVs derived from ginger possess the same characteristics of cytotoxicity and antineoplastic activity. The loaded ginger EVs behave the same compared to aloe and BCS loaded EVs which may mean that the cytotoxicity depicted correlates to the activity of itraconazole in Fig. 7.

Itraconazole is an azole antifungal medication used to treat fungal infections. The cytotoxicity of ITZ was evaluated on HaCat and A172 cell lines using an MTT assay. A dose-dependent and time-dependent reduction

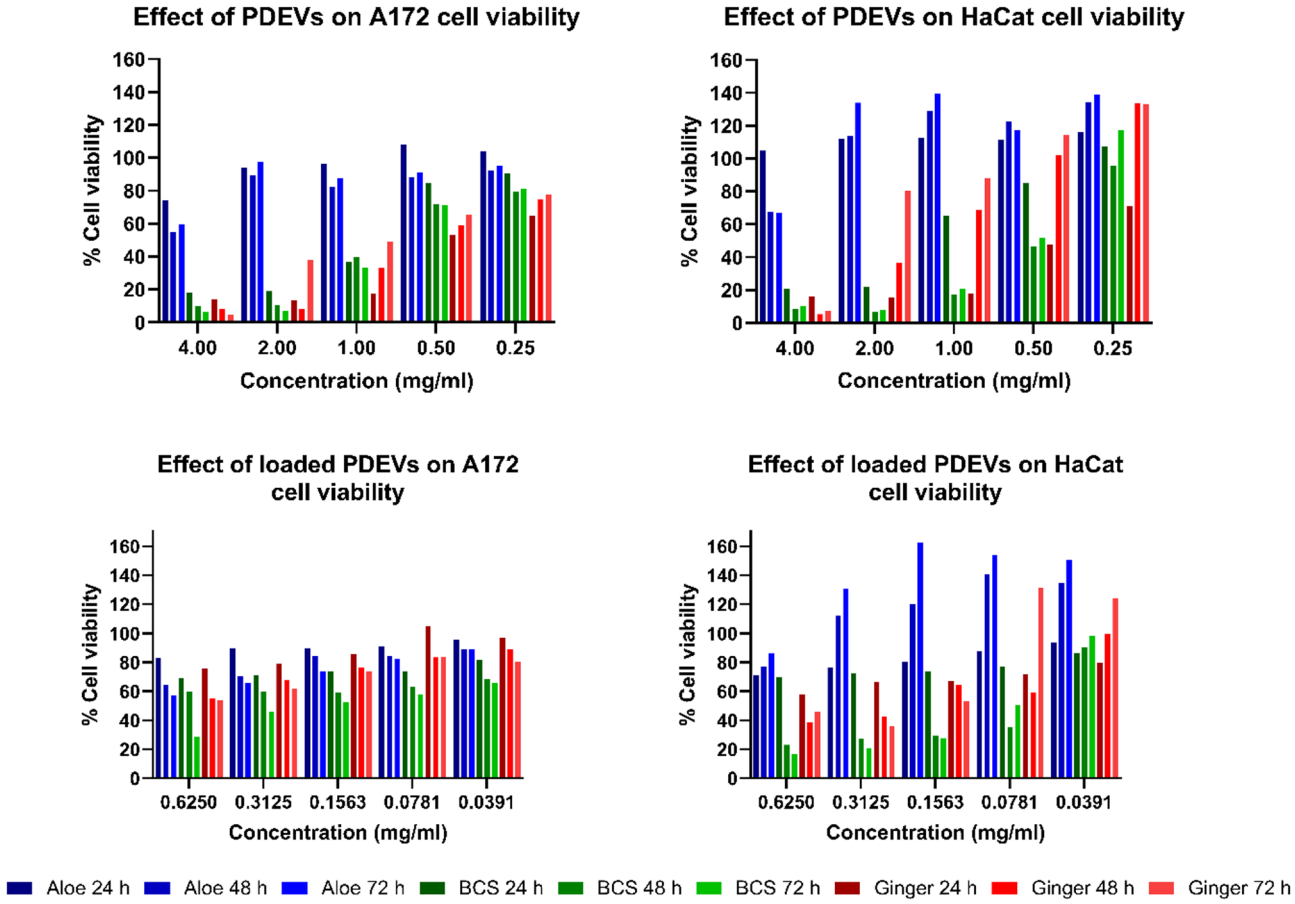

Fig. 7. MTT assay confirming the cytotoxic effect of blank PDEVs and loaded PDEVs on A172 (Glioblastoma) and HaCat (Keratinocytes) cells for 24, 48 and 72 h. (**a**) Effect of blank PDEVs on A172 cell viability, (**b**) Effect of PDEVs on HaCat cell viability, (**c**) Effect of loaded PDEVs on A172 cell viability, and (**d**) Effect of loaded PDEVs on HaCat cell viability.

in cell viability was observed for both cell lines. A172 cells exhibited a more pronounced decrease in viability compared to HaCaT cells across all tested concentrations, suggesting greater sensitivity of the glioblastoma cells to ITZ. Notably, the decline in viability in A172 cells began at lower concentrations and reached below 50% at higher doses, indicating potential anti-cancer efficacy. In contrast, HaCaT cells maintained higher viability across the same concentration range, highlighting a degree of selectivity.

The differential cytotoxic effects of itraconazole suggest a potential therapeutic window for selectively targeting glioblastoma cells. This heightened sensitivity in A172 cells may be attributed to differences in cellular metabolism, membrane composition, or drug uptake mechanisms between cancerous and non-cancerous cells. These findings support the growing interest in repurposing itraconazole as an anti-cancer agent, particularly due to its known inhibition of angiogenesis, Hedgehog signalling, and mTOR (mechanistic target of rapamycin) pathways processes commonly dysregulated in glioblastoma[70]. The relatively lower impact on HaCaT cells indicates a potentially favourable safety profile. Overall, these results warrant further mechanistic investigations and in vivo studies to explore itraconazole's utility as a therapeutic option for glioblastoma. This drug is now researched to repurpose it for the treatment of cancer[71].

Cellular uptake

Fluorescence imaging was carried out as described in the methods section to evaluate cellular uptake of PDEVs and loaded PDEVs by A172 cells. The PDEVs were incubated with FITC for two hours to conjugate the PDEVs. The conjugated PDEVs were exposed to A172 cells for 24 h. Figure 8 shows representative images of the uptake assay of the PDEVs and the loaded PDEVs. The images reveal limited uptake of the blank PDEVs, particularly those derived from aloe, which showed minimal intracellular signal despite being applied at the same concentrations as their drug-loaded and blank PDEVs. In contrast, ITZ loaded PDEVs demonstrated significantly greater uptake across all plant sources, suggesting that drug loading enhances cellular internalization. The improved uptake is likely associated with changes in surface charge, specifically, drug loading resulted in a less anionic zeta potential, which may have enhanced interactions with the negatively charged cell membrane and promoted endocytosis[43]. Glioblastoma (A172) cells in vitro, typically exhibit depolarised resting membrane potentials ranging approximately – 20 to –40 mV in potential[72]. In correlation to PDEVs, ITZ loaded PDEVs have a higher

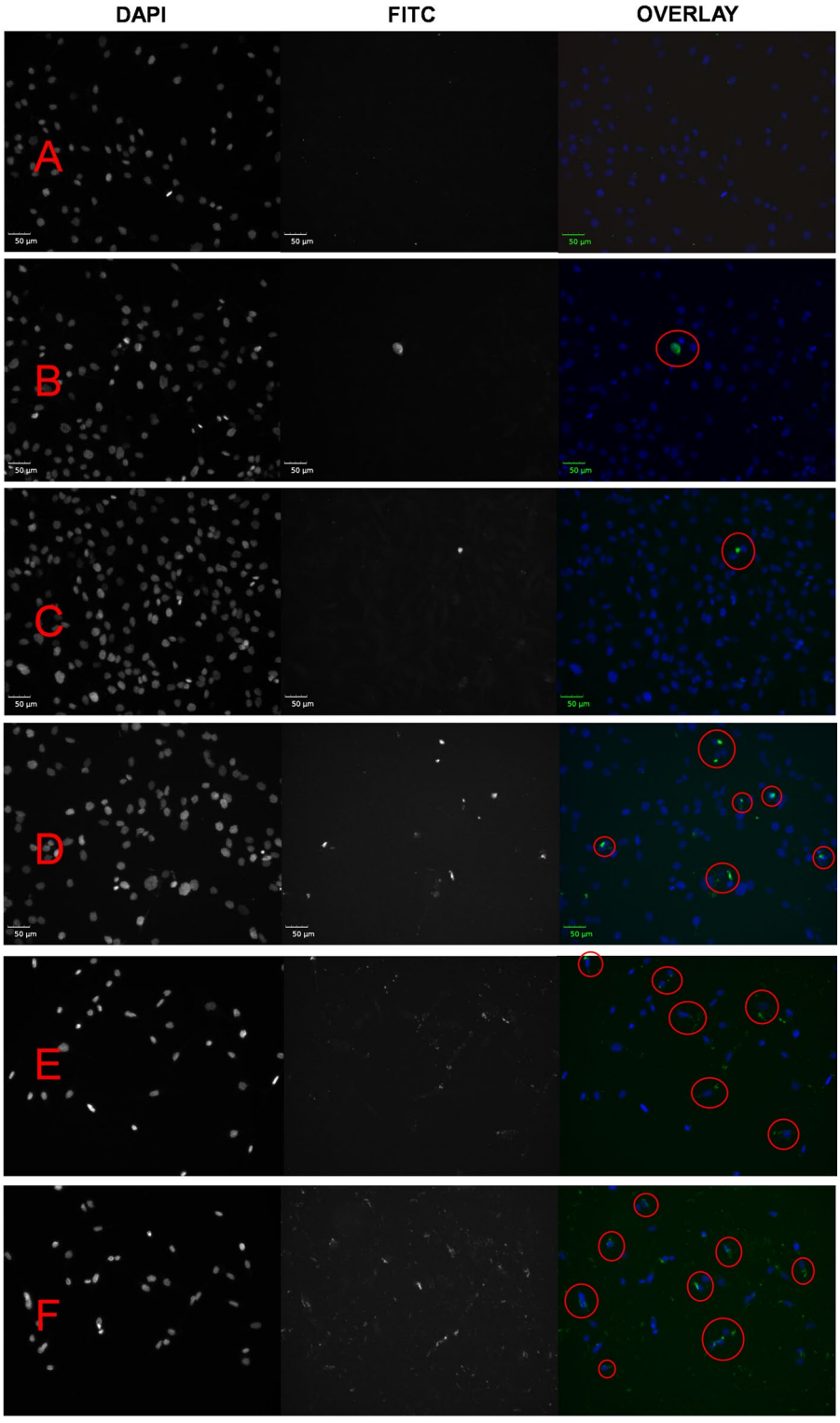

Fig. 8. Cell uptake studies. Fluorescent microscopy images of (**A**) aloe blank EVs, (**B**) BCS blank EVs, (**C**) ginger blank EVs, (**D**) ITZ loaded Aloe EVs, (**E**) ITZ loaded BCS EVs, (**F**) ITZ loaded Ginger EVs.

zeta potential which may increase the electrostatic interaction between the membranes. In contrast, the blank PDEVs, which had a more strongly negative zeta potential were internalized poorly, possibly due to electrostatic repulsion from the cell surface[73]. Interestingly, no major differences were observed in the uptake efficiency among the loaded PDEVs. Hence it is also noted that particle size did not play a dominant role in uptake under the same conditions. Despite the lower concentration of ginger and BCS EVs, fewer viable cells were visibly present, possibly indicating the synergistic cytotoxic effects on the glioblastoma cells as seen in Fig. 7. This also suggests

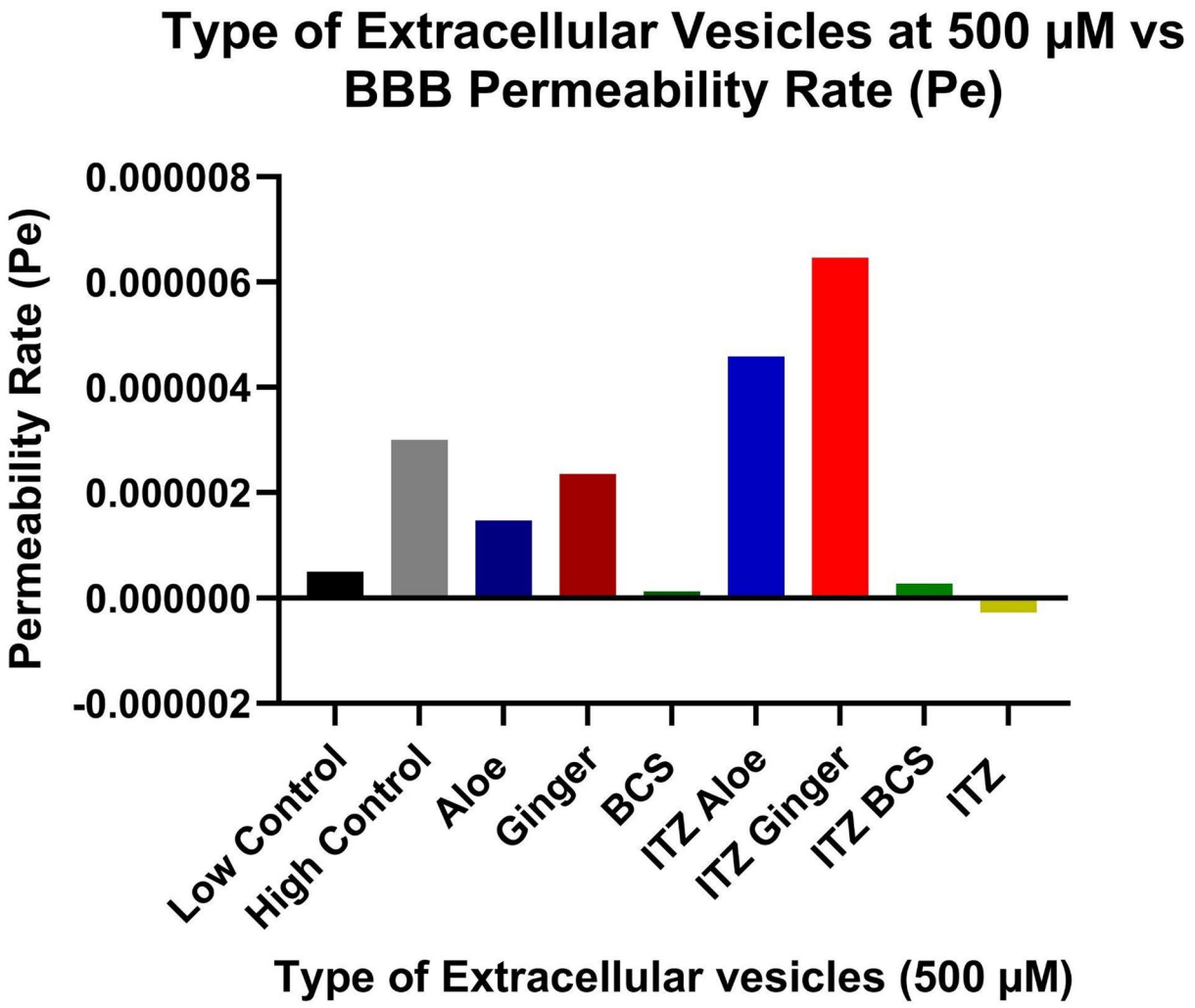

Fig. 9. Assessment of BBB permeation using a permeability rate (Pe) at a constant concentration 500 µM compared to low and high control.

the release of ITZ from the loaded PDEVs through cellular mechanisms impacting cellular internalization. Another important factor affecting uptake visibility may be the FITC-labelling efficiency through different plant sources. FITC is an amine reactive fluorescent probe which labels biomolecules by forming a covalent bond between its isothiocyanate group and the primary and secondary amine groups of the biomolecules[74]. Hence, the exposure of the surface amines varies between each plant as seen in Fig. 3 therefore the FITC binding may also vary through the plant sources.

BBB permeability of the blank and loaded PDEVs

A BBB permeability kit was used to assess the permeability rate of the PDEVs and the loaded PDEVs, as shown in Fig. 9. Permeability rate (Pe), as measured by the BioAssay Systems BBB permeability kit, reflects the capacity of compounds or particles to traverse a model of the BBB. This kit quantifies the apparent permeability coefficient (Pe, in cm/s), providing a comparative measure of how easily a substance crosses the barrier. A higher Pe value indicates greater permeability, while a lower Pe suggests minimal translocation. In this study, three PDEVs were tested both as blank and PDEVs loaded with ITZ. These were compared to kit-provided high and low permeability controls. Ginger blank EVs showed moderately permeability (2.35×10^{-6} cm/s), close to the high control range. Another study was done on ginger constituents to test the BBB permeability which showed that constituents of ginger such as[6]-gingerol[8], -gingerol and[6]-shogaol were able to penetrate the BBB[75]. Aloe blank EVs had a slightly lower but still relatively high permeability (1.47×10^{-6} cm/s). Aloe may have a slight BBB permeability which may be associated with different proteins contained in aloe however there is very limited research done on the BBB permeability of aloe. In contrast, BCS blank EVs exhibited minimal permeability (1.31×10^{-7} cm/s), significantly lower than the low control, indicating poor ability to cross the BBB under basal conditions. This is contradicting as BCS seeds are known to contain thymoquinone which is a low molecular weight lipophilic compound that poses the ability to cross the BBB[76]. Hence, it can be deduced

that the method of extraction and drug loading may not be optimal for BCS blank and loaded EVs reducing its bioactive compound. Ginger and aloe loaded EVs displayed very high permeability rates of 6.46×10^{-6} cm/s and 4.59×10^{-6} cm/s respectively; both exceeding the high control. However, BCS loaded EVs again showed poor permeability (2.76×10^{-7} cm/s), lower than the low permeability control. The results above depict that the extraction and drug loading method of aloe and ginger retains some proteins and lipids that may be beneficial for BBB permeation whilst for BCS, the method of extraction and drug loading may not be optimal.

The pure drug itraconazole was also tested which yielded negligible Pe values, suggesting no measurable permeability in this assay model. These results suggest that the membrane characteristics of aloe and ginger EVs support higher BBB permeability, especially after loading. In contrast, BCS EVs may have membrane composition or lipid/protein degradation that limits translocation, regardless of drug presence.

A concentration gradient study (from 15 to 1000 ug/ml) of the blank and loaded PDEVs was also performed. Aloe and ginger EVs again showed notable permeability trends. Aloe EVs showed slightly variable but generally low Pe values compared to the high control. For the highest concentration of aloe, Pe values were negligible and close to the low control. Ginger EVs had a better permeability across all concentrations with the Pe ranging from 1.0633×10^{-6} to 3.3556×10^{-6} cm/s. BCS had the lowest Pe values suggesting no permeation through the lipid membrane. However, it was noted that the Pe is independent of the concentration of the PDEVs.

Conclusions

In the current study, PDEVs isolated from aloe, ginger and black cumin seeds were fully characterized and comparatively evaluated for their ability to encapsulate highly lipophilic ITZ. Optimisation strategies that could further improve the drug loading capacity include introducing a surfactant for assisted drug loading, optimisation of the temperature during sonication and incubation, pH modification, longer incubation times and higher drug-to-EV ratios to drive higher partitioning and diffusion rate. Results showed that the PDEVs variants were of similar size and zeta potential, however their composition varied, influencing the release mechanism and encapsulation efficiency of ITZ in each case. The PDEVs successfully encapsulated ITZ with steady state zero-order release for the BCS and aloe PDEVs variants. ITZ release from ginger followed the Korsmeyers Peppa model with enhanced uptake by A172 GBM cells. Cell viability studies showed proliferative effects of aloe PDEVs on HaCat cells and cytotoxic effects on the A172 GBM cells. This was not observed at higher concentrations of ginger and BCS PDEVs suggesting toxicity at higher concentration (potential angiogenic effects of PDEVs on GBM cells). PDEVs of ginger had superior BBB permeability over aloe. The BCS variant showed no BBB permeability. In summary, these results provide valuable insight into the use of PDEVs for site-specific delivery of repurposed drugs to treat GBM. As this study serves as a proof of concept for the repurposing of itraconazole using PDEVs for GBM therapy, further formulation development is necessary. Comprehensive stability studies are required to evaluate the long-term physicochemical integrity of the vesicles, including particle size, PDI, zeta potential and drug retention under different storage conditions and in sera. Such evaluation will be essential for determining shelf life, ensuring reproducibility and supporting future translational and in vivo studies. Incorporating these analyses will strengthen the progression of this formulation toward preclinical validation and clinical applicability. Further focus on profiling the lipid, protein and RNA content of the PDEVs will enable engineering strategies for next generation targeting via surface modification to achieve site-specific delivery to brain tissue. Incorporation of these drug-loaded PDEVs with other drug delivery systems, such as intranasal delivery, could enable direct nose-to-brain targeting for GBM – improving patient compliance and enhancing drug availability in the brain with lower administration dosages in such a formulation.

Data availability

All data generated or analysed during this study are included in this manuscript and its supplementary information files.

Received: 22 September 2025; Accepted: 16 December 2025
Published online: 03 January 2026

References

1. Ary Dotiwala, A. K., McCausland, C., Samra Affiliations, N. S. & Anatomy Head and Neck: Blood Brain Barrier.
2. Zhao, Y. et al. Factors influencing the blood-brain barrier permeability. *Brain Res.* https://doi.org/10.1016/j.brainres.2022.147937 (2022).
3. Mathew, E. N., Berry, B. C., Yang, H. W., Carroll, R. S. & Johnson, M. D. Delivering therapeutics to glioblastoma: overcoming biological constraints. *Int. J. Mol. Sci. MDPI*. https://doi.org/10.3390/ijms23031711 (2022).
4. Cha, G. D., Jung, S., Choi, S. H. & Kim, D. H. Local Drug Delivery Strategies for Glioblastoma Treatment. *Brain Tumor Res. Treat.* https://doi.org/10.14791/btrt.2022.0017 (2022).
5. Chen, C. et al. Active cargo loading into extracellular vesicles: Highlights the heterogeneous encapsulation behaviour. *J. Extracell. Vesicles John Wiley Sons Inc* https://doi.org/10.1002/jev2.12163 (2021).
6. Wang, L. et al. MicroRNAs of extracellular vesicles derived from mesenchymal stromal cells alleviate inflammation in dry eye disease by targeting the IRAK1/Table 2/NF-κB pathway. *Ocular Surf. Elsevier Inc.* **28**, 131–140. https://doi.org/10.1016/j.jtos.2023.03.002 (2023).
7. Tajik, T., Baghaei, K., Moghadam, V. E., Farrokhi, N. & Salami, S. A. Extracellular vesicles of cannabis with high CBD content induce anticancer signaling in human hepatocellular carcinoma. *Biomed. Pharmacotherapy Elsevier Masson s r l* https://doi.org/10.1016/j.biopha.2022.113209 (2022).
8. Zhu, J., Wang, S., Yang, D., Xu, W. & Qian, H. Extracellular vesicles: emerging roles, biomarkers and therapeutic strategies in fibrotic diseases. *J. Nanobiotechnol. BioMed. Cent. Ltd.* https://doi.org/10.1186/s12951-023-01921-3 (2023).
9. Herrmann, I. K., Wood, M. J. A. & Fuhrmann, G. Extracellular vesicles as a next-generation drug delivery platform. *Nat. Nanotechnol Nat. Res.* https://doi.org/10.1038/s41565-021-00931-2 (2021).

10. Li, C. et al. Overcoming the blood-brain barrier: exosomes as theranostic nanocarriers for precision neuroimaging. *J. Controlled Release* https://doi.org/10.1016/j.jconrel.2022.08.002 (2022).
11. Cui, L., Perini, G., Palmieri, V., De Spirito, M. & Papi, M. *Plant-derived extracellular vesicles as a novel frontier in cancer therapeutics. nanomaterials* (Multidisciplinary Digital Publishing Institute (MDPI), 2024). https://doi.org/10.3390/nano14161331.
12. Alzahrani, F. A., Khan, M. I., Kameli, N., Alsahafi, E. & Riza, Y. M. *Plant-derived extracellular vesicles and their exciting potential as the future of next-generation drug delivery* (Biomolecules. MDPI, 2023). https://doi.org/10.3390/biom13050839.
13. Bhom, N., Somandi, K., Ramburrun, P. & Choonara, Y. E. *Extracellular nanovesicles as neurotherapeutics for central nervous system disorders. Expert Opin Drug Deliv* (Taylor and Francis Ltd., 2024). https://doi.org/10.1080/17425247.2024.2440099.
14. Ferizi, R., Ramadan, M. F. & Maxhuni, Q. Black seeds (Nigella sativa) medical application and pharmaceutical perspectives. *J. Pharm. Bioallied Sci.* https://doi.org/10.4103/jpbs.jpbs_364_22 (2023).
15. Loggenberg, S. R., Twilley, D., De Canha, M. N., Meyer, D. & Lall, N. The activity of Aloe arborescens miller varieties on wound-associated pathogens, wound healing and growth factor production. *South. Afr. J. Bot. Elsevier B V.* **147**, 1096–1104. https://doi.org/10.1016/j.sajb.2022.04.010 (2022).
16. Shahrajabian, M. H., Sun, W. & Cheng, Q. *Clinical aspects and health benefits of ginger (Zingiber officinale) in both traditional Chinese medicine and modern industry. Acta Agric Scand B Soil Plant Sci* 546–556 (Taylor and Francis Ltd., 2019). https://doi.org/10.1080/09064710.2019.1606930.
17. Kurizaki, A., Watanabe, T. & Devkota, H. P. Chemical constituents from the flowers of Aloe arborescens. *Nat. Prod. Commun. Nat. Prod. Incorporation* https://doi.org/10.1177/1934578X19844135 (2019).
18. Khader, M. & Eckl, P. M. Thymoquinone: an emerging natural drug with a wide range of medical applications.
19. Mao, Q. Q. et al. *Bioactive compounds and bioactivities of ginger (zingiber officinale roscoe). Foods* (MDPI, 2019). https://doi.org/10.3390/foods8060185.
20. Du, S. et al. Extracellular vesicles: a rising star for therapeutics and drug delivery. *J. Nanobiotechnol. BioMed. Cent. Ltd.* https://doi.org/10.1186/s12951-023-01973-5 (2023).
21. Alomari, S. et al. Drug repurposing for glioblastoma and current advances in drug delivery—A comprehensive review of the literature. *Biomolecules MDPI.* https://doi.org/10.3390/biom11121870 (2021).
22. Anwer, M. S., Abdel-Rasol, M. A. & El-Sayed, W. M. Emerging therapeutic strategies in glioblastsoma: drug repurposing, mechanisms of resistance, precision medicine, and technological innovations. *Clin. Exp. Med. Springer Sci. Bus. Media Deutschland GmbH.* https://doi.org/10.1007/s10238-025-01631-0 (2025).
23. In silico drug repurposing: an antifungal drug, itraconazole, repurposed as an anticancer agent using molecular docking.
24. Wirth, F. & Ishida, K. Antifungal drugs: an updated review of central nervous system pharmacokinetics. *Mycoses Blackwell Publishing Ltd.* **63**, 1047–1059. https://doi.org/10.1111/myc.13157 (2020).
25. Lee, H., Park, H., Noh, G. J. & Lee, E. S. pH-responsive hyaluronate-anchored extracellular vesicles to promote tumor-targeted drug delivery. *Carbohydr. Polym. Elsevier Ltd.* **202**, 323–333. https://doi.org/10.1016/j.carbpol.2018.08.141 (2018).
26. Li, Y. J. et al. Gemcitabine loaded autologous exosomes for effective and safe chemotherapy of pancreatic cancer. *Acta Biomater. Acta Mater. Inc.* **101**, 519–530. https://doi.org/10.1016/j.actbio.2019.10.022 (2020).
27. Xi, X. M., Chen-Meng, Xia, S. J. & Lu, R. *Drug loading techniques for exosome-based drug delivery systems. Pharmazie* 61–67 (Govi-Verlag Pharmazeutischer Verlag GmbH, 2021). https://doi.org/10.1691/ph.2021.0128.
28. Malvern Panalytical. Zetasizer Nano ZS User Software (Malvern Panalytical Ltd., Worcestershire, UK). Available at: https://www.malvernpanalytical.com
29. Carl Zeiss Microscopy GmbH.ZEISS SmartSEM Imaging Software. (Carl Zeiss Microscopy GmbH, Cambridge, UK). Available at: https://www.zeiss.com/microscopy
30. Moqejwa, T., Marimuthu, T., Kondiah, P. P. D. & Choonara, Y. E. Development of stable nano-sized transfersomes as a rectal colloid for enhanced delivery of cannabidiol. *Pharm.* https://doi.org/10.3390/pharmaceutics14040703 (2022).
31. Khalbas, A. H., Albayati, T. M., Ali, N. S. & Salih, I. K. Drug loading methods and kinetic release models using of mesoporous silica nanoparticles as a drug delivery system: a review. *Afr. J. Chem. Eng.* https://doi.org/10.1016/j.sajce.2024.08.013 (2024).
32. Waters Corporation. Empower Chromatography Data Software (Waters Corporation, Milford, MA, USA). Available at: https://www.waters.com
33. Rao, Nutan. Stability-indicating method development and validation of itraconazole and terbinafine. *J. Pharm. Clinical. Innovare Acad. Sci. Pvt Ltd.* https://doi.org/10.22159/ajpcr.2019.v12i9.33922 (2019).
34. PerkinElmer Inc. SpectrumTM Software for FT-IR Systems (PerkinElmer Inc., Beaconsfield, UK). Available at: https://www.perkinelmer.com
35. Kim, Y., Park, E. J., Kim, T. W. & Na, D. H. *Recent progress in drug release testing methods of biopolymeric particulate system* (Pharmaceutics. MDPI, 2021). https://doi.org/10.3390/pharmaceutics13081313.
36. Bohrey, S., Chourasiya, V. & Pandey, A. Polymeric nanoparticles containing diazepam: preparation, optimization, characterization, in-vitro drug release and release kinetic study. *Nano Converg Korea Nano Technol. Res. Soc.* https://doi.org/10.1186/s40580-016-0061-2 (2016).
37. Son, G. H., Lee, B. J. & Cho, C. W. Mechanisms of drug release from advanced drug formulations such as polymeric-based drug-delivery systems and lipid nanoparticles. *J. Pharm. Investig Springer Neth.* https://doi.org/10.1007/s40005-017-0320-1 (2017).
38. Hosseini, A. et al. Exosome-inspired targeting of cancer cells with enhanced affinity. *J. Mater. Chem. B Royal Soc. Chem.* **4**, 768–778. https://doi.org/10.1039/c5tb01741f (2016).
39. Ngema, L. M. et al. Surface immobilization of Anti-VEGF peptide on spions for antiangiogenic and targeted delivery of Paclitaxel in Non-Small-Cell lung carcinoma. *ACS Appl. Bio Mater. Am. Chem. Soc.* **6**, 2747–2759. https://doi.org/10.1021/acsabm.3c00224 (2023).
40. Logos Biosystems. CELENA® S Digital Imaging System Software (Logos Biosystems, Gyeonggi-do, South Korea). Available at: https://www.logosbio.com
41. Danaei, M. et al. *Impact of particle size and polydispersity index on the clinical applications of lipidic nanocarrier systems. Pharmaceutics* (MDPI AG, 2018). https://doi.org/10.3390/pharmaceutics10020057.
42. Hersh, A. M., Alomari, S. & Tyler, B. M. Crossing the blood-brain barrier: advances in nanoparticle technology for drug delivery in neuro-oncology. *Int. J. Mol. Sci.* https://doi.org/10.3390/ijms23084153 (2022).
43. Öztürk, K., Kaplan, M. & Çalış, S. Effects of nanoparticle size, shape, and zeta potential on drug delivery. *Int. J. Pharm. Elsevier B V.* https://doi.org/10.1016/j.ijpharm.2024.124799 (2024).
44. Zha, S. et al. *Functionalized Nanomaterials Capable of Crossing the Blood-Brain Barrier* 1820–1845 (ACS Nano. American Chemical Society, 2024). https://doi.org/10.1021/acsnano.3c10674.
45. Golan, M. E. & Stice, S. L. Extracellular vesicle lyophilization for enhanced distribution to the point of care. *Extracell. Vesicle Elsevier BV.* **3**, 100041. https://doi.org/10.1016/j.vesic.2024.100041 (2024).
46. Albakry, Z. et al. Nutritional composition and volatile compounds of Black Cumin (Nigella sativa L.) seed, fatty acid composition and tocopherols, polyphenols, and antioxidant activity of its essential oil. *Horticulturae* https://doi.org/10.3390/horticulturae8070575 (2022).
47. Puia, A. et al. The phytochemical constituents and therapeutic uses of genus aloe: A review. *Not Bot. Horti Agrobot Cluj Napoca Acad. Press.* **49**, 1–16. https://doi.org/10.15835/nbha49212332 (2021).
48. Majid, A. The chemical constituents and Pharmacological effects of Nigella sativa. Journal of bioscience and applied research. *Egypts Presidential Specialized Council Educ. Sci. Res.* **4**, 389–400. https://doi.org/10.21608/jbaar.2018.151793 (2018).

49. Huang, Q., Chen, X., Yu, S., Gong, G. & Shu, H. Research progress in brain-targeted nasal drug delivery. *Front. Aging Neurosci. Front. Media SA*. https://doi.org/10.3389/fnagi.2023.1341295 (2023).
50. Wang, P. et al. Exosomes from M1-polarized macrophages enhance Paclitaxel antitumor activity by activating macrophages-mediated inflammation. *Theranostics Ivyspring Int. Publisher*. **9**, 1714–1727. https://doi.org/10.7150/thno.30716 (2019).
51. Ghadami, S. & Dellinger, K. The lipid composition of extracellular vesicles: applications in diagnostics and therapeutic delivery. *Front. Mol. Biosci. Front. Media SA*. https://doi.org/10.3389/fmolb.2023.1198044 (2023).
52. Li, P., Dai, X., Qu, L., Sui, Y. & Zhang, C. Dual responsive oligo(lysine)-modified pluronic F127 hydrogels for drug release of 5-fluorouracil. *RSC Adv. Royal Soc. Chem.* **10**, 24507–24514. https://doi.org/10.1039/d0ra03207g (2020).
53. Hudiyanti, D., Al Khafiz, M. F., Anam, K., Siahaan, P. & Suyati, L. Assessing encapsulation of Curcumin in cocoliposome: in vitro study. *Open. Chem. De Gruyter Open. Ltd.* **19**, 358–366. https://doi.org/10.1515/chem-2021-0036 (2021).
54. Jovanović, A. A. et al. Design and characterization of liposomal-based carriers for the encapsulation of rosa canina fruit extract. In *Vitro Gastrointestinal Release Behavior. Plants* 13 (Multidisciplinary Digital Publishing Institute (MDPI), 2024). https://doi.org/10.3390/plants13182608.
55. Ghezzi, M. et al. Polymeric micelles in drug delivery: An insight of the techniques for their characterization and assessment in biorelevant conditions. *J. Controlled Release* https://doi.org/10.1016/j.jconrel.2021.02.031 (2021).
56. Lin, X., Yang, H., Su, L., Yang, Z. & Tang, X. Effect of size on the in vitro/in vivo drug release and degradation of exenatide-loaded PLGA microspheres. *J. Drug Deliv Sci. Technol. Editions De Sante*. **45**, 346–356. https://doi.org/10.1016/j.jddst.2018.03.024 (2018).
57. Adepu, S. & Ramakrishna, S. Controlled drug delivery systems: current status and future directions. *Molecules MDPI*. https://doi.org/10.3390/molecules26195905 (2021).
58. Vaz-Salgado, M. A. et al. *Recurrent Glioblastoma: A Review of the Treatment Options. Cancers (Basel)* (Multidisciplinary Digital Publishing Institute (MDPI), 2023). https://doi.org/10.3390/cancers15174279.
59. Lestari, W. A., Wahyuningsih, S., Gomez-Ruiz, S. & Wibowo, F. R. Drug loading ability and release study of various size small mesoporous silica nanoparticle as drug carrier. J Phys Conf Ser. IOP Publishing Ltd; (2022). https://doi.org/10.1088/1742-6596/2190/1/012032
60. Lee, Y. & Thompson, D. H. *Stimuli-responsive liposomes for drug delivery. Wiley Interdiscip Rev Nanomed Nanobiotechnol* (Wiley-Blackwell, 2017). https://doi.org/10.1002/wnan.1450.
61. Cao, L. et al. Extracellular vesicles derived from bone marrow mesenchymal stem cells attenuate dextran sodium sulfate-induced ulcerative colitis by promoting M2 macrophage polarization. *Int. Immunopharmacol. Elsevier B V*. **72**, 264–274. https://doi.org/10.1016/j.intimp.2019.04.020 (2019).
62. Hosonuma, M. & Yoshimura, K. Association between pH regulation of the tumor microenvironment and immunological state. *Front. Oncol. Front. Media SA*. https://doi.org/10.3389/fonc.2023.1175563 (2023).
63. Heredia, N. S. et al. Comparative statistical analysis of the release kinetics models for nanoprecipitated drug delivery systems based on poly(lactic-co-glycolic acid). *PLoS One Public. Libr. Sci.* https://doi.org/10.1371/journal.pone.0264825 (2022).
64. Manirakiza, A., Irakoze, L. & Manirakiza, S. Aloe and its effects on cancer: A Narrative Literature Review [Internet]. www.eahealth.org.
65. Ro, H. S., Jang, H. J., Kim, G. R., Park, S. J. & Lee, H. Y. Enhancement of the Anti-Skin Wrinkling Effects of Aloe arborescens Miller Extracts Associated with Lactic Acid Fermentation. Evidence-based Complementary and Alternative Medicine. Hindawi Limited; ;2020. (2020). https://doi.org/10.1155/2020/2743594
66. Mashayekhi-Sardoo, H., Rezaee, R. & Karimi, G. Nigella sativa (black seed) safety: An overview. *Asian Biomed. Sciendo* https://doi.org/10.1515/abm-2020-0020 (2020).
67. Majdalawieh, A. F. & Fayyad, M. W. Recent advances on the anti-cancer properties of Nigella sativa, a widely used food additive. *J. Ayurveda Integr. Med.* https://doi.org/10.1016/j.jaim.2016.07.004 (2016).
68. Ali, A. M. et al. Cytotoxicity, phytochemical screening and genetic analysis of ginger (Zingiber officinale Rosc.) callus and rhizome. *South. Afr. J. Bot. Elsevier B V*. **151**, 54–59. https://doi.org/10.1016/j.sajb.2021.11.011 (2022).
69. Mohammed, M. et al. In-vitro anticancer and cytotoxic activity of ginger extract on human breast cell lines . *Khartoum J. Pharm. Sci.* **1**(1), 26–29 (2020).
70. Tsubamoto, H. et al. Repurposing itraconazole as an anticancer agent (Review). *Oncol. Lett.* https://doi.org/10.3892/ol.2017.6325 (2017).
71. Isono, R. et al. Itraconazole increases resolvin e3 concentration and 12/15-lipoxygenase inhibitor attenuates Itraconazole cytotoxicity in cervical cancer cells. *Anticancer Res. Int. Inst. Anticancer Res.* **41**, 4271–4276. https://doi.org/10.21873/anticanres.15231 (2021).
72. Molenaar, R. J. Ion channels in glioblastoma. *ISRN Neurol. Hindawi Ltd.* **2011**, 1–7. https://doi.org/10.5402/2011/590249 (2011).
73. Haripriyaa, M. & Suthindhiran, K. Pharmacokinetics of nanoparticles: current knowledge, future directions and its implications in drug delivery. *Futur J. Pharm. Sci. Springer Sci. Bus. Media LLC* https://doi.org/10.1186/s43094-023-00569-y (2023).
74. Shah, D., Guo, Y., Ocando, J. & Shao, J. FITC labeling of human insulin and transport of FITC-insulin conjugates through MDCK cell monolayer. *J. Pharm. Anal. Xi'an Jiaotong Univ.* **9**, 400–405. https://doi.org/10.1016/j.jpha.2019.08.002 (2019).
75. Simon, A., Darcsi, A., Kéry, Á. & Riethmüller, E. Blood-brain barrier permeability study of ginger constituents. *J. Pharm. Biomed. Anal.* https://doi.org/10.1016/j.jpba.2019.112820 (2020).
76. Pottoo, F. H. et al. *Thymoquinone: review of its potential in the treatment of neurological diseases* (Pharmaceuticals. MDPI, 2022). https://doi.org/10.3390/ph15040408.

Author contributions

NB conducted the experiments, analysed the data and was the major contributor in writing this manuscript. PR conceptualized and supervised the research, reviewed and edited this manuscript, and contributed funding support for this research. KZ supervised the research and reviewed and edited this manuscript. YEC conceptualized and supervised the research, reviewed this manuscript, and contributed funding support for this research. All authors read and approved the final manuscript.

Funding

This research was supported by the South African Medical Research Council (SA MRC) under a Self-Initiated Research Grant awarded to Dr Poornima Ramburrun; and the National Research Foundation (NRF) of South Africa under the SARChI Chair program (Grant No. PPNT230823145247), awarded to Prof. Yahya E. Choonara. The views and opinions expressed are those of the author(s) and do not necessarily represent the official views of the SA MRC or NRF.

Declarations

Competing interests
The authors declare no competing interests.

Additional information
Supplementary Information The online version contains supplementary material available at https://doi.org/10.1038/s41598-025-33187-0.

Correspondence and requests for materials should be addressed to Y.E.C.

Reprints and permissions information is available at www.nature.com/reprints.

Publisher's note Springer Nature remains neutral with regard to jurisdictional claims in published maps and institutional affiliations.